



Recent acceleration of Denman Glacier (1972–2017), East Antarctica, driven by grounding line retreat and changes in ice tongue configuration

Bertie W. J. Miles¹, Jim R. Jordan², Chris R. Stokes¹, Stewart S. R. Jamieson¹, G. Hilmar Gudmundsson², and Adrian Jenkins²

¹Department of Geography, Durham University, Durham, DH1 3LE, UK

²Department of Geography and Environmental Sciences, Northumbria University, Newcastle upon Tyne, NE1 8ST, UK

Correspondence: Bertie W. J. Miles (a.w.j.miles@durham.ac.uk)

Received: 16 June 2020 – Discussion started: 6 July 2020

Revised: 9 November 2020 – Accepted: 10 December 2020 – Published: 11 February 2021

Abstract. After Totten, Denman Glacier is the largest contributor to sea level rise in East Antarctica. Denman's catchment contains an ice volume equivalent to 1.5 m of global sea level and sits in the Aurora Subglacial Basin (ASB). Geological evidence of this basin's sensitivity to past warm periods, combined with recent observations showing that Denman's ice speed is accelerating and its grounding line is retreating along a retrograde slope, has raised the prospect that its contributions to sea level rise could accelerate. In this study, we produce the first long-term (~ 50 years) record of past glacier behaviour (ice flow speed, ice tongue structure and calving) and combine these observations with numerical modelling to explore the likely drivers of its recent change. We find a spatially widespread acceleration of the Denman system since the 1970s across both its grounded ($17 \pm 4\%$ acceleration; 1972–2017) and floating portions ($36 \pm 5\%$ acceleration; 1972–2017). Our numerical modelling experiments show that a combination of grounding line retreat, ice tongue thinning and the unpinning of Denman's ice tongue from a pinning point following its last major calving event are required to simulate an acceleration comparable with observations. Given its bed topography and the geological evidence that Denman Glacier has retreated substantially in the past, its recent grounding line retreat and ice flow acceleration suggest that it could be poised to make a significant contribution to sea level in the near future.

1 Introduction

Over the past 2 decades, outlet glaciers along the coastline of Wilkes Land, East Antarctica, have been thinning (Pritchard et al., 2009; Flament and Remy, 2012; Helm et al., 2014; Schröder et al., 2019), losing mass (King et al., 2012; Gardner et al., 2018; Shen et al., 2018; Rignot et al., 2019) and retreating (Miles et al., 2013, 2016). This has raised concerns about the future stability of some major outlet glaciers along the Wilkes Land coastline that drain the Aurora Subglacial Basin (ASB), particularly Totten, Denman, Moscow University and Vanderford glaciers. This is because their present-day grounding lines are close to deep retrograde slopes (Morlighem et al., 2020), meaning there is clear potential for marine ice sheet instability and future rapid mass loss (Weertman, 1974; Schoof, 2007) unless ice shelves provide a sufficient buttressing effect (Gudmundsson, 2013). Geological evidence suggests that there may have been substantial retreat of the ice margin in the ASB during the warm interglacials of the Pliocene (Williams et al., 2010; Young et al., 2011; Aitken et al., 2016; Scherer et al., 2016), which potentially resulted in global mean sea level contributions of up to 2 m from the ASB (Aitken et al., 2016). This is important because these warm periods of the Pliocene may represent our best analogue for climate by the middle of this century under unmitigated emission trajectories (Burke et al., 2018). Indeed, numerical models now predict future sea level contributions from the outlet glaciers which drain the ASB over the coming decades to centuries (Golledge et al., 2015; Ritz et al., 2015; DeConto and Pollard, 2016), but large uncertain-

ties exist over the magnitude and rates of any future sea level contributions.

At present, most studies in Wilkes Land have focused on Totten Glacier, which is losing mass (Li et al., 2016; Mohajerani et al., 2019) in association with grounding line retreat (Li et al., 2015). This has been attributed to wind-forced warm Modified Circumpolar Deep Water accessing the cavity below Totten Ice Shelf (Greenbaum et al., 2015; Rintoul et al., 2016; Greene et al., 2017). However, given our most recent understanding of bedrock topography in Wilkes Land, Denman Glacier (Fig. 1) provides the most direct pathway to the deep interior of the ASB (Gasson et al., 2015; Brancato et al., 2020; Morlighem et al., 2020). Moreover, a recent mass balance estimate (Rignot et al., 2019) has shown that between 1979 and 2017 Denman Glacier's catchment may have lost an amount of ice (190 Gt) broadly comparable with Totten Glacier (236 Gt). There have also been several reports of inland thinning of Denman's fast-flowing trunk (Flament and Remy, 2012; Helm et al., 2014; Young et al., 2015; Schröder et al., 2019), and its grounding line has retreated over the past 20 years (Brancato et al., 2020). However, unlike Totten and other large glaciers which drain marine basins in Antarctica, there has been no detailed study analysing any changes in its calving cycle, velocity or ice tongue structure. This study reports on remotely sensed observations of ice front position and velocity change from 1962 to 2018 and then brings these observations together with numerical modelling to explore the possible drivers of Denman's long-term behaviour. The following section outlines the methods (Sect. 2) used to generate the remote sensing observations (Sect. 3), and we then outline the numerical modelling experiments (Sect. 4) that were motivated by these observations, followed by the discussion (Sect. 5) and conclusion (Sect. 6).

2 Methods

2.1 Ice front and calving cycle reconstruction

We use a combination of imagery from the ARGON (1962), Landsat-1 (1972–1974), Landsat-4–5 (1989–1991), RADARSAT (1997) and Landsat-7–8 (2000–2018) satellites to create a time series of ice front position change from 1962–2018. Suitable cloud-free Landsat imagery was first selected using the Google Earth Engine Digitisation Tool (Lea, 2018). Changes in ice front position were calculated using the box method, which uses an open-ended polygon to take into account any uneven changes along the ice front (Moon and Joughin, 2008). To supplement the large gap in the satellite archive between 1974 and 1989 we use the RESURS KATE-200 space-acquired photography from September 1984. This imagery is hosted by the Australian Antarctic Data Centre, and whilst we could not access the full resolution image, the preview image was sufficient to determine the approximate location of the ice front and confirm

that a major calving event took place shortly before the image was acquired (Fig. S1 in the Supplement).

2.2 Velocity

Maps of glacier velocity between 1972 and 2002 were created using the COSI-Corr (CO-registration of Optically Sensed Images and Correlation) feature-tracking software (Leprince et al., 2007; Scherler et al., 2008). This requires pairs of cloud-free images containing surface features that can be identified in both images. We found three suitable image pairs from the older satellite data: November 1972–February 1974, February 1989–November 1989 and November 2001–December 2002. We used a window size of 128×128 pixels, before projecting velocities onto a WGS 84 grid at a pixel spacing of 1 km.

To reduce noise, we removed all pixels for which ice speed was greater than $\pm 50\%$ of the MEASUREs ice velocity product (Rignot et al., 2011b) and all pixels for which velocity was $< 250 \text{ m yr}^{-1}$. Errors are estimated as the sum of the co-registration error (estimated at 1 pixel) and the error in surface displacement (estimated at 0.5 pixels), which is quantified by comparing computed velocity values to estimates derived from the manual tracking of rifts in the historical imagery (Fig. S2). This resulted in total errors ranging from 20 to 73 m yr^{-1} . Annual estimates of ice speed between 2005–2006 and 2016–2017 were taken from the annual MEASUREs mosaics (Mouginot et al., 2017a). These products are available at a 1 km spatial resolution and are created from the stacking of multiple velocity fields from a variety of sensors between July and June in the following year. To produce the ice speed time series, we extracted the mean value of all pixels within a defined box 10 km behind Denman's grounding line (see Fig. 3). To eliminate any potential bias from missing pixels, we placed boxes in locations where all pixels were present at each time step.

We also estimated changes in the rate of ice front advance between 1962 and 2018. This is possible because inspection of the imagery reveals that there has been only one major calving event at Denman during this time period as the shape of its ice front remained largely unchanged throughout the observation period. Similar methods have been used elsewhere on ice shelves which have stable ice fronts, e.g. Cook East Ice Shelf (Miles et al., 2018). This has the benefit of acting as an independent cross-check on velocities close to the front of the ice tongue that were derived from feature tracking. The ice front advance rate was calculated by dividing ice front position change by the number of days between image pairs. Previous studies (e.g. Miles et al., 2013, 2016; Lovell et al., 2017) have demonstrated that the errors associated with the manual mapping of ice fronts from satellites with a moderate spatial resolution (10–250 m) are typically 1.5 pixels, with co-registration error accounting for 1 pixel and mapping error accounting for 0.5 pixels. This results in ice front advance rate errors ranging from 6 to 73 m yr^{-1} .

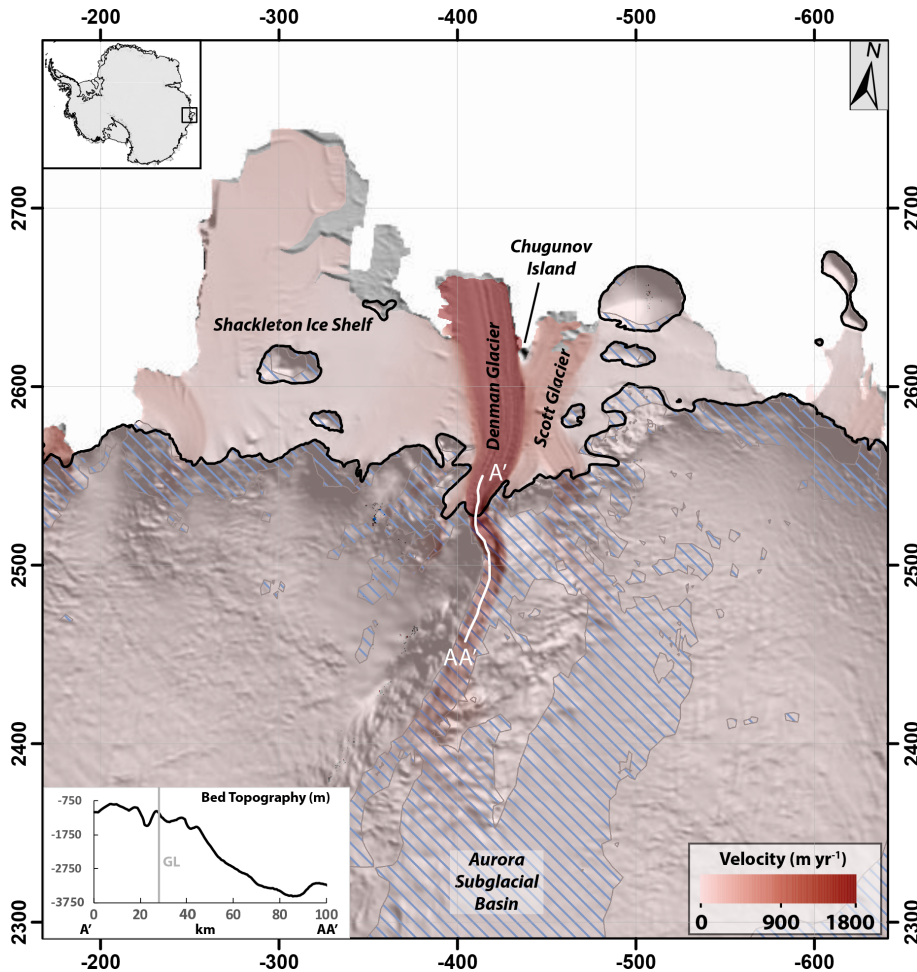


Figure 1. Reference Elevation Model of Antarctica (REMA) mosaic (Howat et al., 2019) of the Denman Glacier and Shackleton Ice Shelf; note the numerous pinning points on the Shackleton Ice Shelf. The MEaSUREs velocity product is overlain (Rignot et al., 2011b), and the grounding line product is from Depoorter et al. (2013). The hatched blue lines represent regions where bedrock elevation is below sea level; note how Denman Glacier drains the Aurora Subglacial Basin. A profile of bedrock elevation from BedMachine (Morlighem et al., 2020) along the transect A'–AA' is located on the bottom left of the figure. Note the reverse bed slope. The coordinates are polar stereographic (km).

The general pattern of ice front advance rates through time is in close agreement with feature-tracking-derived changes in velocity over the same time period.

3 Results

3.1 Ice tongue calving cycles and structure

Throughout our observational record (1962–2018) Denman Glacier underwent only one major calving event in 1984, which resulted in the formation of a large 54 km long (1800 km²) tabular iceberg (Fig. 2). Since this calving event in 1984 the ice front has re-advanced 60 km and there have been no further major calving events (Fig. 2b, c), as indicated by minimal changes to the geometry of its 35 km wide ice front. As of November 2018, Denman Glacier's ice front

was approximately 6 km further advanced than its estimated calving front position immediately prior to the major calving event in 1984 (Fig. 2b, c). However, given the absence of any significant rifting or structural damage, a calving event in the next few years is unlikely. This suggests the next calving event at Denman will take place from a substantially more advanced position (> 10 km) than its last observed event in 1984.

Following the production of the large tabular iceberg from Denman Glacier in 1984, it drifted ~ 60 km northwards before grounding on the sea floor (Fig. 2f) and remained nearly stationary for 20 years before breaking up and dispersing in 2004. Historical observations of sporadic appearances of a large tabular iceberg in this location in 1840 (Cassin and Wilkes, 1858) and 1914 (Mawson, 1915), but not in 1931 (Mawson, 1932), suggest that these low-frequency, high-

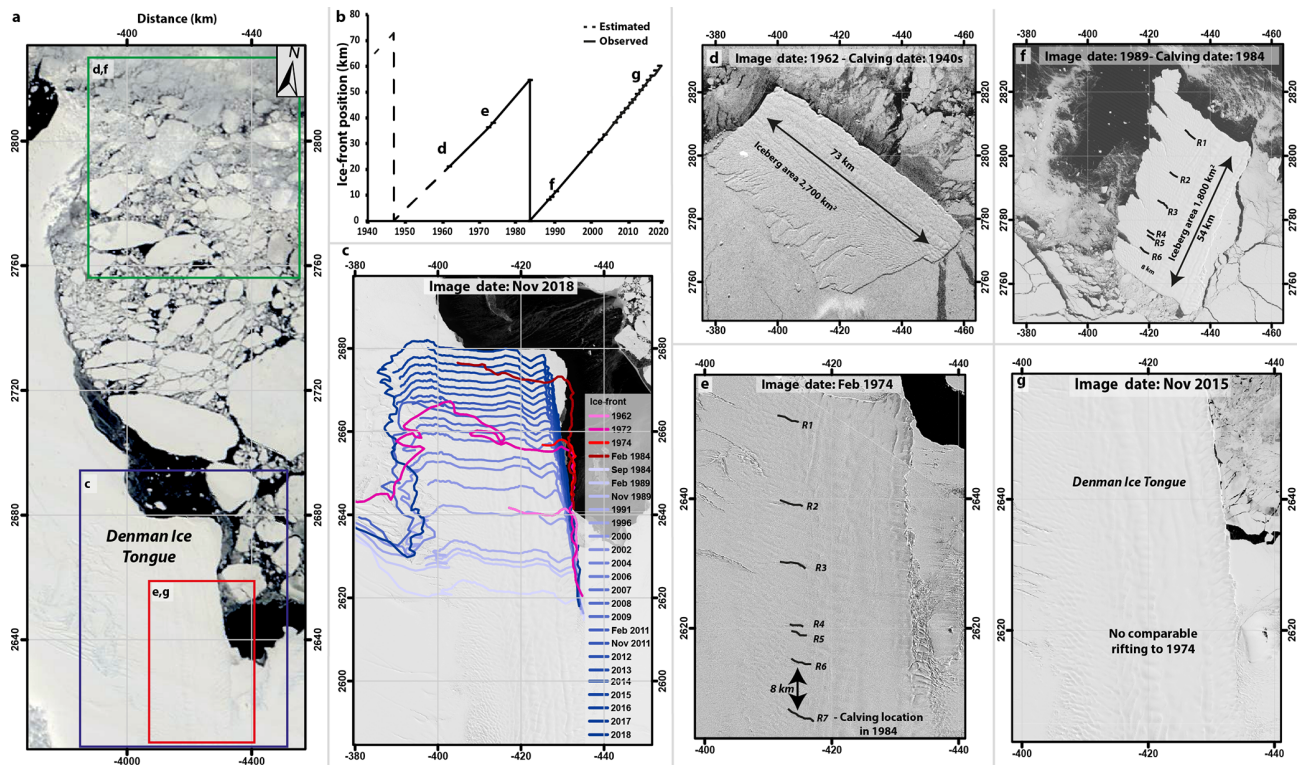


Figure 2. (a) MODIS image from Worldview of the Denman ice tongue in November 2018, with the coloured boxes indicating the locations of panels (c)–(g). (b) Reconstructed calving cycle of Denman Glacier 1940–2018. (c) Examples of ice front mapping 1962–2018. Note the change in the angle of the ice shelf between its present (light blue–dark blue lines) and previous (pink–red lines) calving cycle. (d) ARGON image of a large tabular iceberg in 1962, which likely calved from Denman at some point in the 1940s. (e) Landsat-1 image of the Denman ice tongue in 1972; note the pattern of rifting, which is digitized in black for increased visibility and labelled R1–R7. (f) Landsat-4 image of a large tabular iceberg which calved from Denman in 1984. Note the rifting pattern and the absence of R7, meaning R7 likely propagated during its calving event in 1984. (g) Landsat-8 image of the Denman ice tongue in 2015. Note the absence of rifting. All Landsat images in this figure have been made available courtesy of the U.S. Geological Survey.

magnitude calving events are typical of the long-term behaviour of Denman Glacier. In 1962, our observations indicate a similar large tabular iceberg was present at the same location (Fig. 2d), and, through extrapolation of the ice front advance rate between 1962 and 1974 (Fig. 2b), we estimate that this iceberg was produced at some point in the mid-1940s. However, the iceberg observed in 1962 ($\sim 2700 \text{ km}^2$) was approximately 50 % larger in area than the iceberg produced in 1984 ($\sim 1700 \text{ km}^2$) and 35 % longer (73 km versus 54 km). Thus, whilst Denman’s next calving event will take place from a substantially more advanced position than it did in 1984, it may not be unusual in the context of the longer-term behaviour of Denman Glacier (Fig. 2b).

There are clear differences in the structure of Denman Glacier between successive calving cycles. In all available satellite imagery between the 1940s and the calving event in 1984 (e.g. 1962, 1972 and 1974) an increasing number of rifts (labelled R1 to R7) were observed on its ice tongue throughout this time (Fig. 2e, f). The rifts periodically form $\sim 10 \text{ km}$ inland of Chugunov Island (Fig. 2e), on the western

section of the ice tongue, before being advected down-flow. But a more detailed analysis of how the rifts form is not possible because of the limited availability of satellite imagery in the 1970s and 1980s. An analysis of the rifting pattern in 1974 and the iceberg formed in 1984 indicates that the iceberg calved from R7 (Fig. 2e, f). In contrast, on the grounded iceberg observed in 1962 (Fig. 2d), which likely calved in the 1940s, and in the present-day calving cycle (1984–present; Fig. 2g), similar rifting patterns are not observed.

3.2 Ice speed

We observed widespread increases in ice speed across the entire Denman system between 1972–1974 and 2016–2017, with an overall acceleration of $19 \pm 5 \%$ up to 50 km inland of the grounding line along the main trunk of the glacier (Fig. 3a). Specifically, at box D, 10 km inland of the grounding line, ice flow speed increased by $17 \pm 4 \%$ between 1972–1974 and 2016–2017 (Fig. 3c). The largest rates of acceleration at box D took place between 1972–1974 and 1989 when there was a speed-up of $11 \pm 5 \%$. Between 1989 and

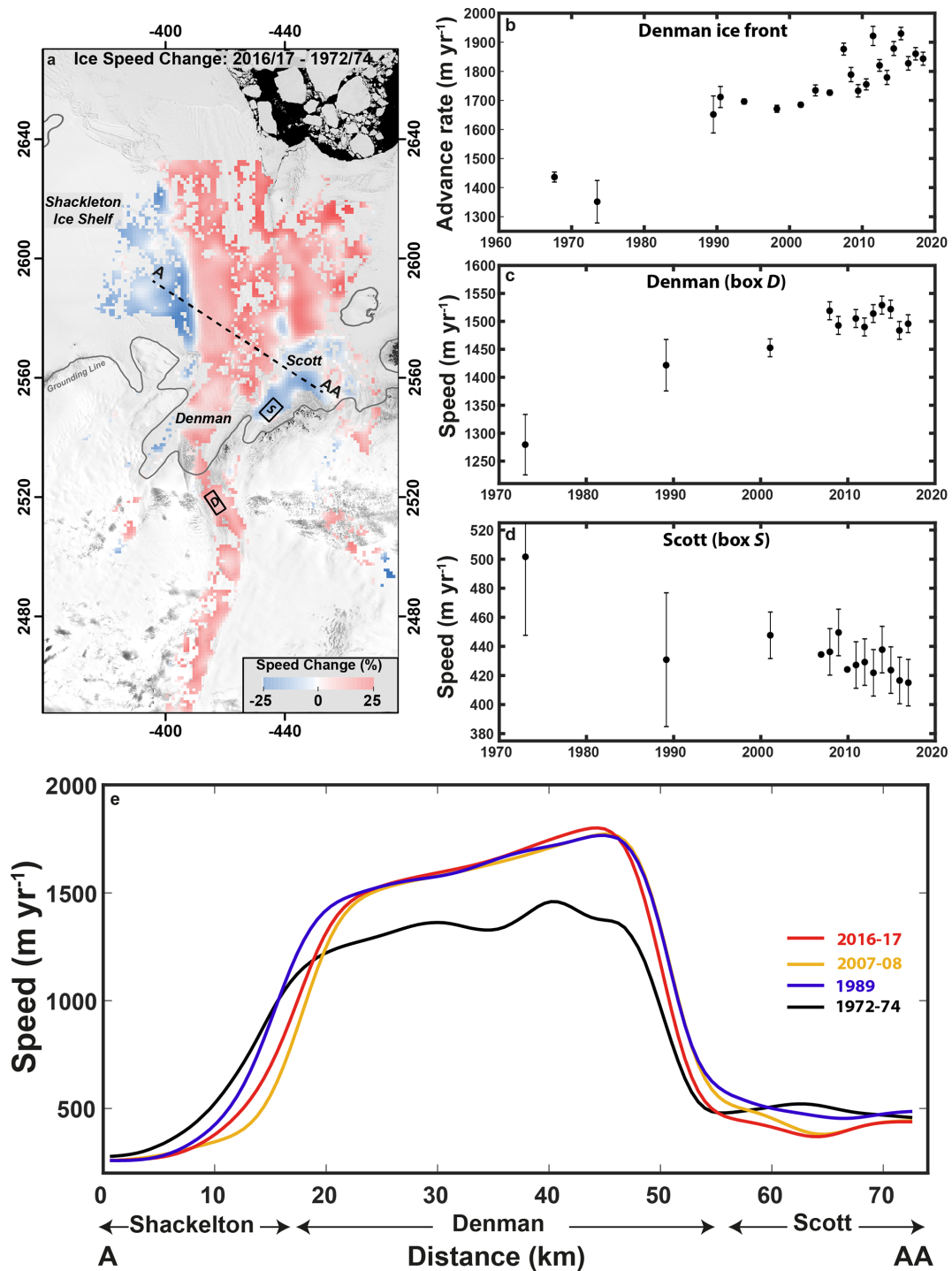


Figure 3. (a) Percentage difference in ice speed between 2016–2017 and 1972–1974 overlain on a Landsat-8 image from November 2017 provided by the U.S. Geological Survey. Red indicates a relative increase in 2016–2017 and blue a relative decrease in 2016–2017. The grounding line is in grey (Depoorter et al., 2013). (b) Time series of the advance rate of the Denman ice front 1962–2018. (c) Time series of mean ice speed from box D, 1972–2017, approximately 10 km behind the Denman grounding line. (d) Time series of mean ice speed from box S on Scott Glacier, 1972–2017. (e) Ice speed profiles across the Shackleton–Denman–Scott system from 1972–1974, 1989, 2007–2008 and 2016–2017. Note the lateral migration of the shear margins.

2016–2017 there was a comparatively slower acceleration of $3 \pm 2\%$ (Fig. 3c). The advance rate of the ice front followed a similar pattern but accelerated at a much greater rate. The ice front advance rate increased by $26 \pm 5\%$ between 1972–1974 and 1989, whilst it increased at a slower rate between 1989 and 2018 ($9 \pm 1\%$; Fig. 3b). At box *S* on the neighbouring Scott Glacier, we observed a $17 \pm 10\%$ decrease in velocity between 1972–1974 and 2016–2017 (Fig. 3d). Similar decreases in ice flow speed are also observed near the shear margin between Shackleton Ice Shelf and Denman Glacier (Fig. 3a, e). The net result of an increase in velocity at Denman Glacier and decreases in velocity on either side of the Shackleton Ice Shelf and Scott Glacier is a steepening of the velocity gradient at the shear margins (Fig. 3e). Ice speed profiles across Denman Glacier also indicate lateral migration of the shear margins of ~ 5 km in both the east and west directions through time (Fig. 3e).

3.3 Lateral migration of Denman’s ice tongue

A comparison of satellite imagery between 1974 and 2002, when Denman’s ice front was in a similar location (e.g. Fig. 4b, c), reveals a lateral migration of its ice tongue and a change in the characteristics of the shear margins. North of Chugunov Island, towards the ice front, we observe a bending and westward migration of the ice tongue in 2002 compared to its 1974 position (Fig. 4b, c). In 1974, the ice tongue was intensely shearing against Chugunov Island, as indicated by the heavily damaged shear margins (Fig. 4d). However, by 2002 the ice tongue made substantially less contact with Chugunov Island because this section of the ice tongue migrated westwards (Fig. 4d, e). South of Chugunov Island there was a greater divergence of flow between the Denman and Scott glaciers in 2002 compared to 1974, resulting in a more damaged shear margin (Fig. 4d, e). On the western shear margin between Shackleton Ice Shelf and Denman’s ice tongue there was no obvious change in structure between 1974 and 2002 (Fig. 4f, g). However, velocity profiles in this region show an eastward migration of the fast-flowing ice tongue (Fig. 3e).

4 Numerical modelling

4.1 Model set-up and experimental design

To help assess the possible causes of the acceleration of Denman Glacier since 1972 and the importance of changes we observe on Denman’s ice tongue, we conduct diagnostic numerical modelling experiments using the finite-element ice dynamics model $\dot{U}a$ (Gudmundsson et al., 2012). $\dot{U}a$ is used to solve the equations of the shallow ice stream or “shelfy stream” approximation (SSA; Cuffey and Paterson, 2010). This can be expressed for one horizontal dimension as

$$2\partial_x \left(A^{-\frac{1}{n}} h (\partial_x u)^{\frac{1}{n}} \right) - GC^{-\frac{1}{m}} u^{\frac{1}{m}} = \rho g h \partial_x s + \frac{1}{2} g h^2 \partial_x \rho,$$

Table 1. Summary of the perturbations included in each of our seven numerical modelling experiments.

Experiment	Ice shelf thinning	Grounding line retreat	Unpinning from Chugunov Island
E1	✓		
E2		✓	
E3	✓	✓	
E4			✓
E5	✓		✓
E6		✓	✓
E7	✓	✓	✓

where A is the rate factor with its corresponding stress factor n , h is the vertical ice thickness, G is a grounding–flotation mask (1 for grounded ice, 0 for floating ice), C is the basal slipperiness with its corresponding stress exponent m , ρ is the density of ice and g is the acceleration due to gravity. Previously, the model has been used to understand rates and patterns of grounding line migration and glacier responses to ice shelf buttressing and ice shelf thickness (e.g. Reese et al., 2018; Hill et al., 2018; Gudmundsson et al., 2019), and it has been involved in several model intercomparison experiments (e.g. Pattyn et al., 2008, 2012; Leverman et al., 2020).

Modelled ice velocities are calculated on a finite-element grid using a vertically integrated form of the momentum equations. The model domain consists of 93 371 elements with horizontal dimensions ranging from 250 m near the grounding line to 10 km further inland. Zero-flow conditions are applied along the inland boundaries, chosen to match zero-flow contours from observations. The relationship between creep and stress is assumed to follow Glen’s flow law using stress exponent $n = 3$, and basal sliding is assumed to follow Weertman’s sliding law, with its own stress exponent, $m = 3$. Other modelling parameters related to ice rheology and basal conditions are the basal slipperiness, C , and the rate factor, A . We initialized the ice flow model by changing both the ice rate factor A (Fig. S3b) and basal slipperiness C (Fig. S3c) using an inverse approach (Vogel, 2002) and iterating until the surface velocities of the numerical model closely matched the 2009 measurements of ice flow (Fig. S3).

4.2 Perturbation experiments

To ascertain the most likely causes of the observed acceleration for Denman Glacier we start from a baseline set-up representing the ice shelf in 2009, when both ice geometry and velocity are well known, and compare to diagnostic simulations of reconstructed 1972 ice geometry. We chose 2009 for this baseline set-up because the calving front is in approximately the same position as in 1972 when our glacier observations start, thus ruling out any acceleration in response to a change in ice front extent. We use the BedMachine (Morlighem et al., 2020) ice thickness, bathymetry and

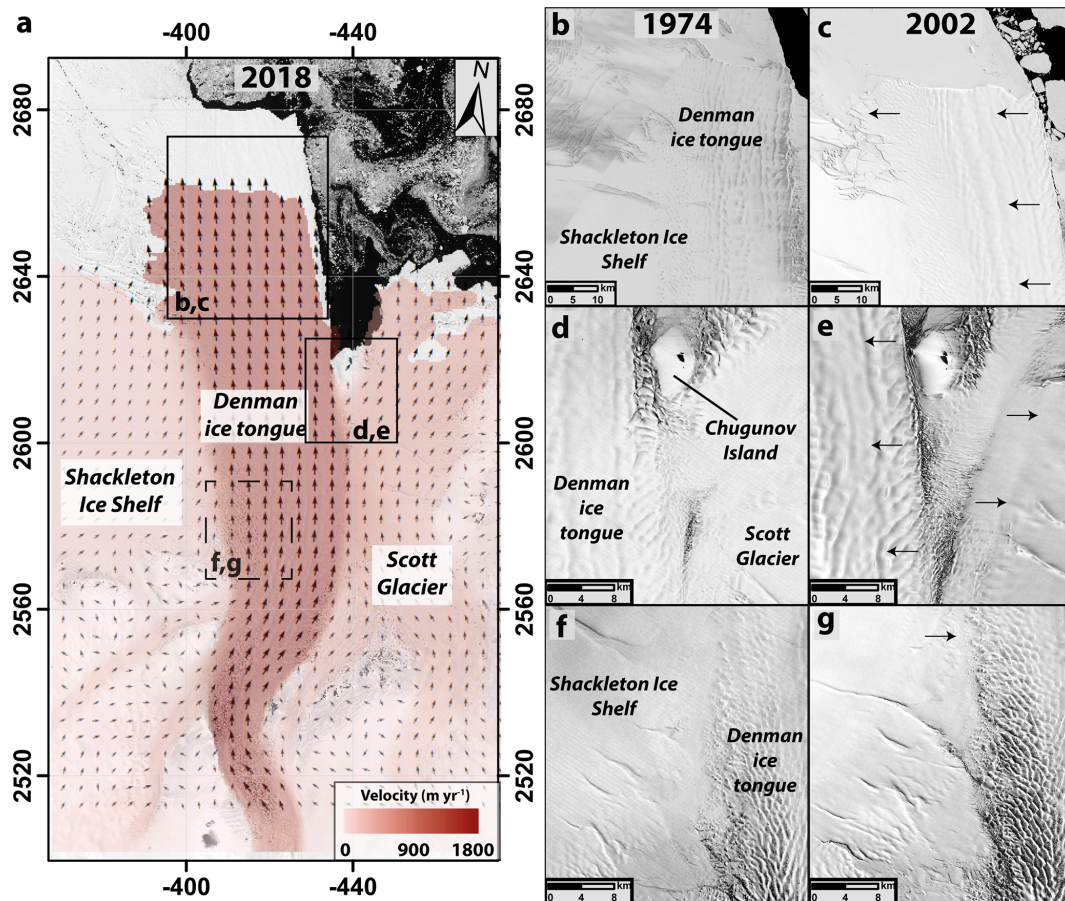


Figure 4. (a) Landsat-8 image overlain with MEaSUREs velocity vectors (Rignot et al., 2011b). (b, d, f) Close-up examples of ice tongue structure and position from a Landsat-1 image in 1974. (c, e, g) Close-up examples of ice tongue structure and position from a Landsat-7 image in 2002. In particular, note the reduction in contact between Denman Glacier and Chugunov Island between 1974 (d) and 2002 (e). The arrows in panels (c), (e) and (g) represent the direction of migration of the Denman ice tongue since 1974. All Landsat images in this figure have been made available courtesy of the U.S. Geological Survey.

grounding line position and MEaSUREs ice velocities for 2009 (Mouginot et al., 2017a) as inputs. The baseline simulation is then perturbed to test its response to a series of potential drivers that may be responsible for the observed changes in ice geometry since the 1970s. Specifically, we apply observation-based perturbations to test Denman’s response to ice shelf thinning (i), grounding line retreat (ii) and the unpinning of Denman’s ice tongue from Chugunov Island (iii), which are detailed below.

- i. To represent ice shelf thinning since 1972, we take the mean annual rate of ice thickness change from the 1994–2012 ice shelf thickness change dataset (Paolo et al., 2015) and scale it up to represent the total thickness change over the 37 years between 1972 and 2009, assuming that the 1994–2012 mean annual rate remains constant during this period. This thickness change is then applied to the 2009 ice geometry, which is modified to better represent the estimated 1972 ice thickness distribution of the Shackleton Ice Shelf, Denman

ice tongue and Scott Glacier. Similar to the methodology of Gudmundsson et al. (2019), we only apply this thickness change to fully floating nodes, with no change in ice thickness for grounded ice and ice directly over the grounding line. The total thickness change applied is shown in Fig. S4. We refer to this perturbation as “ice shelf thinning” because the majority of the floating portions of Denman’s ice tongue and Shackleton Ice Shelf have thinned since 1994, although some sections of Scott Glacier have actually thickened near its calving front (Fig. S4).

- ii. In the Úa ice model, the grounding line position is not explicitly defined by the user but is instead a direct result of ice thickness, bedrock depth, and the relative densities of ice and seawater. As such, the two ways to perturb a given grounding line are to modify either the ice thickness or the bedrock depth. Modifying the bedrock depth is the less disruptive approach because

the resulting effect upon velocity is not biased by an imposed change in ice thickness at the grounding line affecting the regional ice velocity field due to flux conservation, in addition to that caused by shifting the grounding line. Note that raising the bedrock to meet the underside of the ice shelf in this way is not a representation of any real Earth processes; it is merely forcing the model to have the grounding line in a particular location that then enables a diagnostic simulation. To represent grounding line retreat since 1972 we advanced Denman's grounding line from its position in the 2009 baseline set-up by 10 km to a possible 1972 position. This is achieved by raising the bedrock approximately ~ 20 – 30 m in the area shown in Fig. S4. We justify a 10 km retreat since 1972 based on the rate of grounding line retreat observed between 1996 and 2017 (~ 5 km; Brancato et al., 2020). For the newly grounded area, values of the bed slipperiness, C , are not generated in our model inversion; we therefore prescribe nearest-neighbour values to those at the grounding line in the model inversion.

- iii. To represent the pinning of Denman's ice tongue against Chugunov Island in the 1972 observations (e.g. Fig. 4d, e), we artificially raise a small area of bedrock on the western edge of Chugunov Island (Fig. S4). Bed slipperiness was set to a value comparable to that immediately upstream of the grounding line. Note that, although past observations suggest that the ice in front of Chugunov Island has been damaged, possibly having an effect on its rate factor, A , we have decided to limit our investigation to the effect of pinning the ice on Chugunov Island without changing the rate factor. To properly investigate the possible change in past rate factor we would need less spatially patchy 1972 velocities and an accurate understanding of past ice geometry (itself an unknown under investigation) to perform a model inversion for 1972 conditions.

These three adjustments are applied, both individually and in combination with each other, to the baseline model set-up to produce seven different simulations (E1–7), summarized in Table 1, which respectively perturb the following:

- E1. ice shelf thinning,
- E2. grounding line retreat,
- E3. ice shelf thinning and grounding line retreat,
- E4. unpinning from Chugunov Island,
- E5. ice shelf thinning and unpinning from Chugunov Island,
- E6. grounding line retreat and unpinning from Chugunov Island, and
- E7. ice shelf thinning, grounding line retreat and unpinning from Chugunov Island.

Below we compare the instantaneous change in ice velocity arising from each perturbation experiment to observed changes in velocity, and then we use these comparisons to understand the relative importance of each process in contributing to Denman's behaviour over the past 50 years.

4.3 Model results

We show observed 2009 ice speed relative to each of the seven simulations which represent possible 1972 ice geometries (E1–7, Fig. 5b–h). In all cases, positive (red) values indicate areas where ice was flowing faster and negative (blue) values show areas where ice was flowing slower in 2009 relative to each 1972 simulation. Perturbing ice shelf thickness to represent ice shelf thinning since the 1970s results in higher velocities over both the grounded and floating portions of the Denman system (E1, Fig. 5b). However, the simulated acceleration on Denman's ice tongue (E1, Fig. 5b) is much larger than the observed acceleration, with the simulation showing a 50 % acceleration in the area just downstream of the grounding line compared to the observed 20 % acceleration between 1972 and 2009 (E1, Fig. 5b). Thus, it would appear that ice shelf thinning alone is not consistent with the observed velocity changes in the Denman system. Perturbing the grounding line to account for a possible grounding line retreat since 1972 simulates changes in ice flow speeds comparable to observations near Denman's grounding line (E2, Fig. 5c), but it is unable to reproduce the observed increases in ice speed across Denman's ice tongue (E2, Fig. 5c). Thus, grounding line retreat alone is also unable to reproduce the observed pattern of velocity changes. Ice shelf thinning and retreating the grounding line result in very similar patterns in ice speed change (E3, Fig. 5d) to that of the grounding line retreat perturbation experiment (E2).

In isolation, simulating the unpinning of Denman's ice tongue from Chugunov Island has a very limited effect on ice flow speeds, with no change in speed near the grounding line and a very spatially limited change on the ice tongue (E4; Fig. 5e). However, when combining the unpinning perturbation with either ice shelf thinning (E5; Fig. 5f) or grounding line retreat (E6; Fig. 5g), it is clear that the unpinning from Chugunov Island causes an acceleration across Denman's ice tongue. For E5 this results in an even larger overestimate of ice speed change across Denman's ice tongue in comparison to experiment 1, which only perturbs ice shelf thickness. However, for experiment 6 the additional inclusion of the unpinning from Chugunov Island to grounding line retreat results in a simulated pattern of ice flow speed change very similar to observations. Specifically, the unpinning from Chugunov Island has caused an acceleration across the ice tongue that was not present in experiment 2. Combining all three perturbations (E7, Fig. 5h) produces changes in ice velocity that are most comparable to observations. Both the spatial pattern in ice speed change and the simulated ice speed within box D (Fig. 5i) are very similar to observations

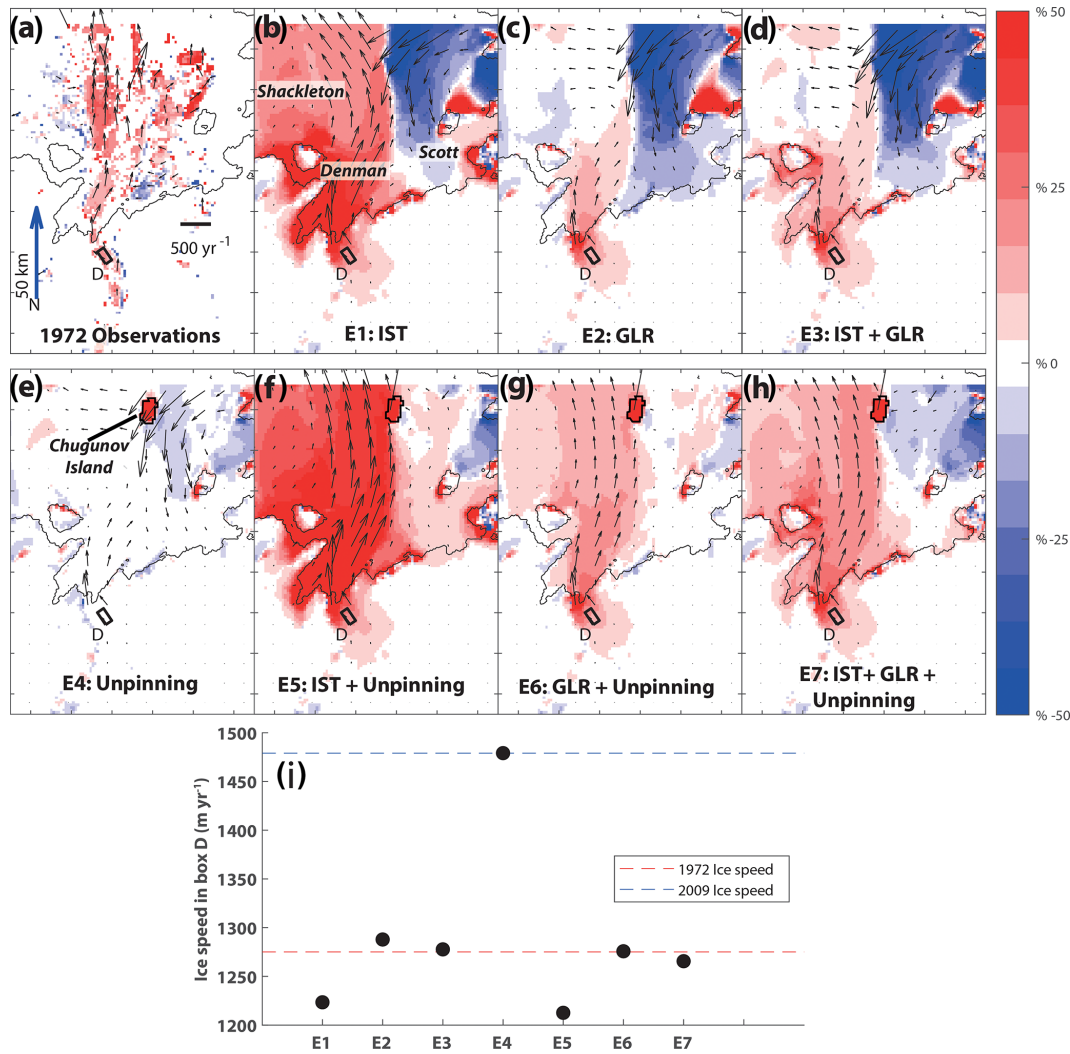


Figure 5. The effect of varying ice geometry on ice flow: ice velocity difference between 2009 observations and (a) observations from 1972; (b–h) seven experiments which perturb 2009 ice geometry to represent possible 1972 ice geometry configurations. In each experiment combinations of ice shelf thinning (IST), grounding line retreat (GLR) and the unpinning from Chugunov Island are perturbed (see Table 1). Note that red indicates areas where ice flowed faster in 2009, and blue indicates areas flowing slower, with arrows showing the direction and magnitude of change when compared to the 1972 perturbations. (i) Mean speed from box D in each experiment; the dotted red line represents the observed mean speed from box D in 1972, and the blue line represents observed speed from 2009. E7 most closely matches the speed observed in box D, the spatial pattern of the observed acceleration and the westward bending of Denman’s ice tongue.

for both experiments, and the enhanced westward bending of the directional component of ice velocity in experiment E7 is more consistent with the observed westward bending of the ice tongue (e.g. Fig. 2b).

5 Discussion

5.1 Variation in Denman Glacier’s calving cycle

Our calving cycle reconstruction, combined with historical observations (Cassin and Wilkes, 1858; Mawson, 1915, 1932), hints that Denman’s multi-decadal high-magnitude

calving cycle has remained broadly similar over the past 200 years. It periodically produces a large tabular iceberg, which then drifts ~ 60 km northwards before grounding on an offshore ridge and typically remains in place for around 20 years before disintegrating and/or dispersing. However, more detailed observations and reconstructions of its past three calving events have shown that there are clear differences in both the size of icebergs produced and in ice tongue structure through time (Fig. 2). The large variation (50 %) in both the size of icebergs produced and the location the ice front calved from indicates variability in its calving cycle.

Extending observational records for ice shelves that calve at irregular intervals, sizes or locations is especially im-

portant because it helps to distinguish between changes in glacier dynamics caused by longer-term variations in its calving cycle and changes in glacier dynamics forced by climate. For example, there have been large variations in ice flow speed at the Brunt Ice Shelf over the past 50 years (Gudmundsson et al., 2017), but these large variations can be explained by internal processes following interactions with local pinning points during the ice shelf's calving cycle (Gudmundsson et al., 2017). In contrast, the widespread acceleration of outlet glaciers in the Amundsen Sea sector (Mouginot et al., 2014) is linked to enhanced intrusions of warm ocean water increasing basal melt rates (e.g. (Thoma et al., 2008; Jenkins et al., 2018), leading to ice shelf thinning (Paolo et al., 2015) and grounding line retreat (Rignot et al., 2011a). Thus, in the following section we discuss whether the observed speed-up of Denman since the 1970s (Fig. 3) is more closely linked to variations in its calving cycle (e.g. Brunt Ice Shelf) or if it has been driven by climate and ocean forcing (e.g. Amundsen Sea).

5.2 What has caused Denman Glacier's acceleration since the 1970s?

We observe a spatially widespread acceleration of both Denman's floating and grounded ice. This is characterized by a $17 \pm 4\%$ increase in ice flow speed near the grounding line between 1972 and 2017 (Fig. 3c) and a $36 \pm 5\%$ acceleration in ice front advance rate from 1972–2017, or a $30 \pm 5\%$ increase in the ice front advance rate between 1962 and 2017 (Fig. 3b). Our estimates of the acceleration of the ice front advance rate are of a comparable magnitude to the 36% acceleration of the ice tongue between 1957 and 2017 based on averaged point estimates across the ice tongue from repeat aerial surveys (Dolgushin, 1966; Rignot et al., 2019). Taken together, this suggests a limited change in ice tongue speed between 1957 and 1972, before a rapid acceleration between 1972 and 2017. However, the rate of acceleration throughout this period has not been constant (Fig. 3b, c). Between 1972 to 1990, observations indicate that ice accelerated $26 \pm 5\%$ on the ice tongue (Fig. 3b) and $11 \pm 5\%$ at the grounding line (Fig. 3c) in comparison to more limited accelerations of $9 \pm 1\%$ and $3 \pm 2\%$, respectively, between 1990 and 2017. When comparing these observations against our numerical modelling experiments we find that grounding line retreat, changes in ice shelf thickness and the unpinning of ice from Chugunov Island (Fig. 5h) are all required to explain an acceleration of a comparable magnitude and spatial pattern across the Denman system.

Averaged basal melt rates across the Shackleton–Denman system are comparable to the Getz Ice Shelf (Depoorter et al., 2013; Rignot et al., 2013). Close to Denman's deep grounding line, melt rates have been estimated at 45 m yr^{-1} (Brancato et al., 2020), suggesting the presence of modified Circumpolar Deep Water in the ice shelf cavity. At nearby Totten Glacier (Fig. 1a), wind-driven periodic intrusions of warm

water flood the continental shelf and cause increased basal melt rates (Rintoul et al., 2016; Greene et al., 2017) and grounding line retreat (Li et al., 2015). It is possible that a similar process may be responsible for some of the observed changes at Denman Glacier. Hydrographic data collected from the Marine Mammals Exploring the Oceans Pole to Pole consortium (Treasure et al., 2017) show water temperatures of -1.31 to -0.26°C at depths between 550 and 850 m on the continental shelf in front of Denman (Brancato et al., 2020). Thus, whilst not confirmed, there is clear potential for warm water to reach Denman's grounding zone and enhance melt rates.

Recent observations of grounding line migration at Denman have shown a 5 km retreat along its western flank between 1996 and 2017 (Brancato et al., 2020). However, over this time period there was a limited change in the speed of Denman (2001–2017; $3 \pm 2\%$ acceleration; Fig. 3c), and our time series indicates that the acceleration initiated earlier at some point between 1972 and 1990 (Fig. 3c). Reconstructions of the bed topography near the grounding line of Denman Glacier show that the western flank of Denman's grounding line was resting on a retrograde slope in 1996 a few kilometres behind a topographic ridge (Brancato et al., 2020). One possibility is that Denman's grounding line retreat initiated much earlier at some point in the 1970s in response to increased ocean temperatures enhancing melting of the ice tongue base. This initial grounding line retreat and possible ocean-induced ice tongue thinning may have caused the initial rapid acceleration between 1972 and 1990, before continuing at a slower rate. However, our numerical modelling shows that whilst the combination of the retreat of Denman's grounding line and ice tongue thinning can produce a magnitude of acceleration near the grounding line similar to observations (E3; Fig. 5d), these modelled processes cannot explain the widespread acceleration across the ice tongue (e.g. E4; Fig. 5e).

In order to simulate a comparable spatial acceleration across both Denman's grounded and floating ice to observations, the unpinning of ice from Chugunov Island following Denman's last calving event in 1984 is required (e.g. E6 and 7; Fig. 5g, h). In isolation, the reduction in contact with Chugunov Island has had no effect on ice flow speeds at both Denman's grounding line and ice tongue (E4; Fig. 5e). However, when combined with grounding line retreat and ice tongue thinning, the spatial pattern of simulated ice speed change across the ice tongue more closely resemble observations (E6 and 7; Fig. 5g, h). Specifically, the unpinning of the ice tongue from Chugunov Island has caused an acceleration across much of Denman's ice tongue. The most likely explanation as to why the unpinning from Chugunov Island only influences ice speed patterns in combination with ice tongue thinning and grounding line retreat, and not in isolation, is that ice tongue thinning and grounding line retreat have caused a change in the direction of flow of the ice tongue since the 1970s. In all simulations that perturb either

ice tongue thickness or retreat the grounding line (Fig. 5b, c, e, f, g, h), there is a clear westward bending in ice flow direction near Chugunov Island, which results in a reduction in contact between the ice tongue and Chugunov Island. This is consistent with observations that show a distinctive westward bending of Denman's ice tongue since the 1970s (Fig. 2b). These findings therefore suggest that the reduction in contact with Chugunov Island following Denman's calving event in 1984 caused an instantaneous acceleration across large sections of its ice tongue, meaning that this calving event had a direct impact on the spatial pattern of acceleration observed between 1972 and 2017. However, because of the westward bending of Denman's ice tongue during its re-advance following its 1984 calving event, the ice tongue now makes limited contact with Chugunov Island (e.g. Fig. 4e) and has a very limited effect on ice flow speeds (e.g. E4; Fig. 5e).

The acceleration of Denman's ice tongue following its last major calving event in 1984 may have also caused a series of positive feedbacks, resulting in further acceleration. We observe a steepening of the velocity gradient across Denman's shear margins, a pattern of acceleration of the dominant Denman ice tongue, and a slowdown of the neighbouring Shackleton Ice Shelf and Scott Glacier (Fig. 3a). We also observe the lateral migration of the shear margins at sub-decadal timescales (Fig. 3e). These distinctive patterns in ice speed change are very similar to those reported at the Stancomb–Wills Ice Shelf (Humbert et al., 2009) and between the Thwaites Ice Tongue and Eastern Ice Shelf (Mouginot et al., 2014; Miles et al., 2020); they are symptomatic of a weakening of shear margins. Therefore, we suggest that at Denman, after the initial acceleration following the reduction in contact with Chugunov Island, the shear margins may have weakened, causing further acceleration. We do not include this process in our numerical experiments, and it may explain the divergence between observations and simulated ice speed change in the neighbouring Shackleton Ice Shelf and Scott Glacier (Figs. 3a, 5).

Overall, our observations and numerical simulations suggest that the cause of Denman's acceleration since the 1970s is complex and likely reflects a combination of processes linked to the ocean and a reconfiguration of Denman's ice tongue. One possibility is that the acceleration of ice across Denman's grounding line has almost entirely been driven by warm ocean forcing driving grounding line retreat and ice tongue thinning, with the unpinning of Denman's ice tongue from Chugunov Island only causing a localized acceleration across floating ice. An alternative explanation is that warm ocean forcing has caused ice tongue thinning and grounding line retreat, but the acceleration behind the grounding line has been enhanced through time by changes in ice tongue configuration. Either way, our results highlight the fact that both oceanic processes and the changes in ice tongue structure associated with Denman's calving event have been important in causing Denman's observed acceleration.

5.3 Future evolution of Denman Glacier

In the short term, an important factor in the evolution of the wider Denman–Shackleton system is Denman's next calving event. Whilst our observations do not suggest that a calving event is imminent (next 1–2 years), our calving cycle reconstruction indicates that a calving event at some point in the 2020s is highly likely. Because the calving cycle of Denman Glacier has demonstrated some variability in the past (e.g. Fig. 2), the precise geometry of its ice tongue after this calving event cannot be accurately predicted. In particular, it is unclear how Denman's ice tongue will realign in relation to Chugunov Island following its next calving event. For example, if following Denman's next calving event the direction of ice flow shifts eastwards to a similar configuration to the 1970s and the ice tongue makes contact with Chugunov Island, the increased resistance could slow down Denman's ice tongue for the duration of its calving cycle, but it is unclear if any slowdown could propagate to the grounding line. Thus, this calving event may have important implications for the evolution of the Denman–Shackleton system for multiple decades because it could influence both ice flow speed and direction.

In the medium term (next 50 years) atmospheric warming could also have a direct impact on the stability of the Denman–Shackleton system. Following the collapse of Larsen B in 2002, Shackleton is now the most northerly major ice shelf remaining in Antarctica, with most of the ice shelf lying outside the Antarctic Circle. Numerous surface meltwater features have been repeatedly reported on its surface (Kingslake et al., 2017; Stokes et al., 2019; Arthur et al., 2020). There is no evidence that these features currently have a detrimental impact on its stability, but there is a possibility that projected increases in surface melt (Trusel et al., 2015) could increase the ice shelves' vulnerability to meltwater-induced hydrofracturing.

6 Conclusion

We have reconstructed Denman Glacier's calving cycle to show that its previous two calving events (\sim 1940s and 1984) varied in size by 50 %, and there have been clear differences in ice tongue structure, with a notable unpinning from Chugunov Island following the 1984 calving event. We also observe a long-term acceleration of Denman Glacier across both grounded and floating sections of ice, with both the ice front advance rate and ice near the grounding line accelerating by 36 ± 5 % and 17 ± 4 %, respectively, between 1972 and 2017. We show that in order to simulate a post-1972 acceleration that is comparable with observations, its grounding line must have retreated since the 1970s. We also highlight the importance of the reconfiguration of the Denman ice tongue system in determining the spatial pattern of acceleration observed.

The recent changes in the Denman system are important because Denman's grounding line currently rests on a retrograde slope which extends 50 km into its basin (Morlighem et al., 2020; Brancato et al., 2020), suggesting clear potential for marine ice sheet instability. Given the large catchment size, it has potential to make globally significant contributions to mean sea level rise in the coming decades (1.49 m; Morlighem et al., 2020). Crucial to assessing the magnitude of any future sea level contributions is improving our understanding of regional oceanography and determining whether the observed changes at Denman are the consequence of a longer-term ocean warming. This is in addition to monitoring and understanding the potential impact of any future changes in the complex Shackleton–Denman ice shelf system.

Code and data availability. Landsat and the declassified historical imagery from 1962 is freely available and can be downloaded via Earth Explorer (<https://earthexplorer.usgs.gov/>, last access: 1 February 2020). COSI-Corr is available at http://www.tectonics.caltech.edu/slip_history/spot_coseis/download_software.html (last access: 1 February 2020). The source code for Úa is available at <https://doi.org/10.5281/zenodo.3706624> (Gudmundsson, 2020). MEaSUREs annual ice velocity maps are available at <https://doi.org/10.5067/9T4EPQXTJYW9> (Mouginot et al., 2017b). The historical ice velocities and ice front shapefiles are available at <https://doi.org/10.5285/42504802-313C-4F7C-AC8C-104EF9B4E077> (Miles et al., 2021).

Supplement. The supplement related to this article is available online at: <https://doi.org/10.5194/tc-15-663-2021-supplement>.

Author contributions. All authors contributed to the design of the study. BWJM collected and analysed the remote sensing data. JRJ undertook the numerical modelling. BWJM led the paper writing with input from all authors.

Competing interests. The authors declare that they have no conflict of interest.

Acknowledgements. Landsat imagery was provided free of charge by the US Geological Survey Earth Resources Observation Science Center. We also acknowledge the use of imagery from the NASA Worldview application (<https://worldview.earthdata.nasa.gov/>, last access: 1 February 2020), part of the NASA Earth Observing System Data and Information System (EOSDIS). We also thank Eric Rignot for providing digitized estimates of ice flow speed across parts of Denman's ice tongue based on the mapped estimates of Dolgushin (1966). We would like to thank Chad Greene and two anonymous reviewers, along with the editor Bert Wouters, for providing constructive comments which led to the improvement of this paper.

Financial support. This research has been supported by NERC (grant no. NE/R000824/1).

Review statement. This paper was edited by Bert Wouters and reviewed by Chad Greene and two anonymous referees.

References

- Aitken, A. R. A., Roberts, J. L., van Ommen, T. D., Young, D. A., Golledge, N. R., Greenbaum, J. S., Blankenship, D. D., and Siegert, M. J.: Repeated large-scale retreat and advance of Totten Glacier indicated by inland bed erosion, *Nature*, 533, 385–389, 2016.
- Arthur, J. F., Stokes, C. R., Jamieson, S. S. R., Carr, J. R., and Lee-son, A. A.: Distribution and seasonal evolution of supraglacial lakes on Shackleton Ice Shelf, East Antarctica, *The Cryosphere*, 14, 4103–4120, <https://doi.org/10.5194/tc-14-4103-2020>, 2020.
- Brancato, V., Rignot, E., Milillo, P., Morlighem, M., Mouginot, J., An, L., Scheuchl, B., Jeong, S., Rizzoli, P., Bueso Bello, J. L., and Prats-Iraola, P.: Grounding line retreat of Denman Glacier, East Antarctica, measured with COSMO-SkyMed radar interferometry data, *Geophys. Res. Lett.*, 47, e2019GL086291, <https://doi.org/10.1029/2019GL086291>, 2020.
- Burke, K. D., Williams, J. W., Chandler, M. A., Haywood, A. M., Lunt, D. J., and Otto-Bliesner, B. L.: Pliocene and Eocene provide best analogs for near-future climates, *P. Natl. Acad. Sci. USA*, 115, 13288–13293, 2018.
- Cassin, J. and Wilkes, C.: United States Exploring Expedition: During the Years 1838, 1839, 1840, 1841, 1842, Under the Command of Charles Wilkes, USN. Mammalogy and Ornithology, JB Lippincott & Company, Philadelphia, 1858.
- Cuffey, K. M. and Paterson, W. S. B.: The physics of glaciers, Fourth edition, Amsterdam, J. Glaciol., 57, 383–384, <https://doi.org/10.3189/002214311796405906>, 2010.
- DeConto, R. M. and Pollard, D.: Contribution of Antarctica to past and future sea-level rise, *Nature*, 531, 591–597, 2016.
- Depoorter, M. A., Bamber, J. L., Griggs, J. A., Lenaerts, J. T. M., Ligtenberg, S. R. M., van den Broeke, M. R., and Moholdt, G.: Calving fluxes and basal melt rates of Antarctic ice shelves, *Nature*, 502, 89–92, 2013.
- Dolgushin, L. D.: New data on the rates of movement of Antarctic glaciers, *Soviet Antarctic Expedition Information Bulletin*, 55, 41–42, 1966.
- Flament, T. and Remy, F.: Dynamic thinning of Antarctic glaciers from along-track repeat radar altimetry, *J. Glaciol.*, 58, 830–840, 2012.
- Gardner, A. S., Moholdt, G., Scambos, T., Fahnestock, M., Ligtenberg, S., van den Broeke, M., and Nilsson, J.: Increased West Antarctic and unchanged East Antarctic ice discharge over the last 7 years, *The Cryosphere*, 12, 521–547, <https://doi.org/10.5194/tc-12-521-2018>, 2018.
- Gasson, E., DeConto, R., and Pollard, D.: Antarctic bedrock topography uncertainty and ice sheet stability, *Geophys. Res. Lett.*, 42, 5372–5377, 2015.
- Golledge, N. R., Kowalewski, D. E., Naish, T. R., Levy, R. H., Fogwill, C. J., and Gasson, E. G. W.: The multi-millennial Antarctic commitment to future sea-level rise, *Nature*, 526, 421–425, 2015.

- Greenbaum, J. S., Blankenship, D. D., Young, D. A., Richter, T. G., Roberts, J. L., Aitken, A. R. A., Legresy, B., Schroeder, D. M., Warner, R. C., van Ommen, T. D., and Siegert, M. J.: Ocean access to a cavity beneath Totten Glacier in East Antarctica, *Nat. Geosci.*, 8, 294–298, 2015.
- Greene, C. A., Blankenship, D. D., Gwyther, D. E., Silvano, A., and van Wijk, E.: Wind causes Totten Ice Shelf melt and acceleration, *Sci. Adv.*, 3, e1701681, 2017.
- Gudmundsson, H.: GHilmarG/UaSource: Ua2019b (Version v2019b), Zenodo, <https://doi.org/10.5281/zenodo.3706624>, 2020.
- Gudmundsson, G. H.: Ice-shelf buttressing and the stability of marine ice sheets, *The Cryosphere*, 7, 647–655, <https://doi.org/10.5194/tc-7-647-2013>, 2013.
- Gudmundsson, G. H., Krug, J., Durand, G., Favier, L., and Gagliardini, O.: The stability of grounding lines on retrograde slopes, *The Cryosphere*, 6, 1497–1505, <https://doi.org/10.5194/tc-6-1497-2012>, 2012.
- Gudmundsson, G. H., de Rydt, J., and Nagler, T.: Five decades of strong temporal variability in the flow of Brunt Ice Shelf, Antarctica, *J. Glaciol.*, 63, 164–175, 2017.
- Gudmundsson, G. H., Paolo, F. S., Adusumilli, S., and Fricker, H. A.: Instantaneous Antarctic ice-sheet mass loss driven by thinning ice shelves, *Geophys. Res. Lett.*, 46, 13903–13909, <https://doi.org/10.1029/2019GL085027>, 2019.
- Helm, V., Humbert, A., and Miller, H.: Elevation and elevation change of Greenland and Antarctica derived from CryoSat-2, *The Cryosphere*, 8, 1539–1559, <https://doi.org/10.5194/tc-8-1539-2014>, 2014.
- Hill, E. A., Gudmundsson, G. H., Carr, J. R., and Stokes, C. R.: Velocity response of Petermann Glacier, northwest Greenland, to past and future calving events, *The Cryosphere*, 12, 3907–3921, <https://doi.org/10.5194/tc-12-3907-2018>, 2018.
- Howat, I. M., Porter, C., Smith, B. E., Noh, M.-J., and Morin, P.: The Reference Elevation Model of Antarctica, *The Cryosphere*, 13, 665–674, <https://doi.org/10.5194/tc-13-665-2019>, 2019.
- Humbert, A., Kleiner, T., Mohrholz, C. O., Oelke, C., Greve, R., and Lange, M. A.: A comparative modeling study of the Brunt Ice Shelf/Stancomb-Wills Ice Tongue system, East Antarctica, *J. Glaciol.*, 55, 53–65, 2009.
- Jenkins, A., Shoosmith, D., Dutrieux, P., Jacobs, S., Kim, T. W., Lee, S. H., Ha, H. K., and Stammerjohn, S.: West Antarctic Ice Sheet retreat in the Amundsen Sea driven by decadal oceanic variability, *Nat. Geosci.*, 11, 733–738, 2018.
- King, M. A., Bingham, R. J., Moore, P., Whitehouse, P. L., Bentley, M. J., and Milne, G. A.: Lower satellite-gravimetry estimates of Antarctic sea-level contribution, *Nature*, 491, 586–589, 2012.
- Kingslake, J., Ely, J. C., Das, I., and Bell, R. E.: Widespread movement of meltwater onto and across Antarctic ice shelves, *Nature*, 544, 349–352, 2017.
- Lea, J. M.: The Google Earth Engine Digitisation Tool (GEEDiT) and the Margin change Quantification Tool (MaQiT) – simple tools for the rapid mapping and quantification of changing Earth surface margins, *Earth Surf. Dynam.*, 6, 551–561, <https://doi.org/10.5194/esurf-6-551-2018>, 2018.
- Leprince, S., Ayoub, F., Klinger, Y., and Avouac, J. P.: Co-Registration of Optically Sensed Images and Correlation (COSI-Corr): an operational methodology for ground deformation measurements, *Igarss: 2007 IEEE International Geoscience and Remote Sensing Symposium*, 1–12, 1943–1946, <https://doi.org/10.1109/Igarss.2007.4423207>, 2007.
- Levermann, A., Winkelmann, R., Albrecht, T., Goelzer, H., Gollledge, N. R., Greve, R., Huybrechts, P., Jordan, J., Leguy, G., Martin, D., Morlighem, M., Pattyn, F., Pollard, D., Quiquet, A., Rodehacke, C., Seroussi, H., Sutter, J., Zhang, T., Van Breedam, J., Calov, R., DeConto, R., Dumas, C., Garbe, J., Gudmundsson, G. H., Hoffman, M. J., Humbert, A., Kleiner, T., Lipscomb, W. H., Meinshausen, M., Ng, E., Nowicki, S. M. J., Perego, M., Price, S. F., Saito, F., Schlegel, N.-J., Sun, S., and van de Wal, R. S. W.: Projecting Antarctica’s contribution to future sea level rise from basal ice shelf melt using linear response functions of 16 ice sheet models (LARMIP-2), *Earth Syst. Dynam.*, 11, 35–76, <https://doi.org/10.5194/esd-11-35-2020>, 2020.
- Li, X., Rignot, E., Morlighem, M., Mouginit, J., and Scheuchl, B.: Grounding line retreat of Totten Glacier, East Antarctica, 1996 to 2013, *Geophys. Res. Lett.*, 42, 8049–8056, 2015.
- Li, X., Rignot, E., and Mouginit, J.: Ice flow dynamics and mass loss of Totten Glacier, East Antarctica, from 1989 to 2015, *Geophys. Res. Lett.*, 43, 6366–6373, 2016.
- Lovell, A., Stokes, C., and Jamieson, S.: Sub-decadal variations in outlet glacier terminus positions in Victoria Land, Oates Land and George V Land, East Antarctica (1972–2013), *Antarct. Sci.*, 29, 468–483, 2017.
- Mawson, D.: *The Home of the Blizzard*, Heinemann, London, 1915.
- Mawson, D.: *The BANZ Antarctic Research Expedition, 1929–31*, *Geograph. J.*, 80.2, 101–126, 1932.
- Miles, B., Jordan, J., Stokes, C., Jamieson, S., Gudmundsson, G. H., and Jenkins, A.: Ice front position and velocities for Denman Glacier 1962–2018, Polar Data Centre, Natural Environment Research Council, UK Research & Innovation, <https://doi.org/10.5285/42504802-313c-4f7c-ac8c-104ef9b4e077>, 2021.
- Miles, B. W. J., Stokes, C. R., Vieli, A., and Cox, N. J.: Rapid, climate-driven changes in outlet glaciers on the Pacific coast of East Antarctica, *Nature*, 500, 563–566, 2013.
- Miles, B. W. J., Stokes, C. R., and Jamieson, S. S. R.: Pan-ice-sheet glacier terminus change in East Antarctica reveals sensitivity of Wilkes Land to sea-ice changes, *Sci. Adv.*, 2, e1501350, 2016.
- Miles, B. W. J., Stokes, C. R., and Jamieson, S. S. R.: Velocity increases at Cook Glacier, East Antarctica, linked to ice shelf loss and a subglacial flood event, *The Cryosphere*, 12, 3123–3136, <https://doi.org/10.5194/tc-12-3123-2018>, 2018.
- Miles, B. W. J., Stokes, C. R., Jenkins, A., Jordan, J. R., Jamieson, S. S. R., and Gudmundsson, G. H.: Intermittent structural weakening and acceleration of the Thwaites Glacier Tongue between 2000 and 2018, *J. Glaciol.*, 66, 485–495, 2020.
- Mohajerani, Y., Velicogna, I., and Rignot, E.: Evaluation of Regional Climate Models Using Regionally Optimized GRACE Mascons in the Amery and Getz Ice Shelves Basins, Antarctica, *Geophys. Res. Lett.*, 46, 13883–13891, 2019.
- Moon, T. and Joughin, I.: Changes in ice front position on Greenland’s outlet glaciers from 1992 to 2007, *J. Geophys. Res.-Earth*, 113, F02022, 2008.
- Morlighem, M., Rignot, E., Binder, T., Blankenship, D., Drews, R., Eagles, G., Eisen, O., Ferraccioli, F., Forsberg, R., Fretwell, P., Goel, V., Greenbaum, J. S., Gudmundsson, H., Guo, J. X., Helm, V., Hofstede, C., Howat, I., Humbert, A., Jokat, W., Karlsson, N. B., Lee, W. S., Matsuoka, K., Millan, R., Mouginit, J., Paden,

- J., Pattyn, F., Roberts, J., Rosier, S., Ruppel, A., Seroussi, H., Smith, E. C., Steinhage, D., Sun, B., van den Broeke, M. R., van Ommen, T. D., van Wessem, M., and Young, D. A.: Deep glacial troughs and stabilizing ridges unveiled beneath the margins of the Antarctic ice sheet, *Nat. Geosci.*, 13, 132–137, 2020.
- Mouginot, J., Rignot, E., and Scheuchl, B.: Sustained increase in ice discharge from the Amundsen Sea Embayment, West Antarctica, from 1973 to 2013, *Geophys. Res. Lett.*, 41, 1576–1584, 2014.
- Mouginot, J., Rignot, E., Scheuchl, B., and Millan, R.: Comprehensive Annual Ice Sheet Velocity Mapping Using Landsat-8, Sentinel-1, and RADARSAT-2 Data, *Remote Sens.-Basel*, 9, 364, 2017a.
- Mouginot, J., Scheuchl, B., and Rignot, E.: MEaSUREs Annual Antarctic Ice Velocity Maps 2005–2017, Version 1, Boulder, Colorado USA, NASA National Snow and Ice Data Center Distributed Active Archive Center, <https://doi.org/10.5067/9T4EPQXTJYW9>, 2017b.
- Paolo, F. S., Fricker, H. A., and Padman, L.: Volume loss from Antarctic ice shelves is accelerating, *Science*, 327–331, <https://doi.org/10.1126/science.aaa0940>, 2015.
- Pattyn, F., Perichon, L., Aschwanden, A., Breuer, B., de Smedt, B., Gagliardini, O., Gudmundsson, G. H., Hindmarsh, R. C. A., Hubbard, A., Johnson, J. V., Kleiner, T., Kononov, Y., Martin, C., Payne, A. J., Pollard, D., Price, S., Rückamp, M., Saito, F., Souček, O., Sugiyama, S., and Zwinger, T.: Benchmark experiments for higher-order and full-Stokes ice sheet models (ISMIP-HOM), *The Cryosphere*, 2, 95–108, <https://doi.org/10.5194/tc-2-95-2008>, 2008.
- Pattyn, F., Schoof, C., Perichon, L., Hindmarsh, R. C. A., Bueler, E., de Fleurian, B., Durand, G., Gagliardini, O., Gladstone, R., Goldberg, D., Gudmundsson, G. H., Huybrechts, P., Lee, V., Nick, F. M., Payne, A. J., Pollard, D., Rybak, O., Saito, F., and Vieli, A.: Results of the Marine Ice Sheet Model Intercomparison Project, MISIP, *The Cryosphere*, 6, 573–588, <https://doi.org/10.5194/tc-6-573-2012>, 2012.
- Pritchard, H. D., Arthern, R. J., Vaughan, D. G., and Edwards, L. A.: Extensive dynamic thinning on the margins of the Greenland and Antarctic ice sheets, *Nature*, 461, 971–975, 2009.
- Reese, R., Gudmundsson, G. H., Levermann, A., and Winkelmann, R.: The far reach of ice-shelf thinning in Antarctica, *Nat. Clim. Change*, 8, 53–57, 2018.
- Rignot, E., Mouginot, J., and Scheuchl, B.: Antarctic grounding line mapping from differential satellite radar interferometry, *Geophys. Res. Lett.*, 38, L10504, 2011a.
- Rignot, E., Mouginot, J., and Scheuchl, B.: Ice Flow of the Antarctic Ice Sheet, *Science*, 333, 1427–1430, 2011b.
- Rignot, E., Jacobs, S., Mouginot, J., and Scheuchl, B.: Ice-Shelf Melting Around Antarctica, *Science*, 341, 266–270, 2013.
- Rignot, E., Mouginot, J., Scheuchl, B., van den Broeke, M., van Wessem, M. J., and Morlighem, M.: Four decades of Antarctic Ice Sheet mass balance from 1979–2017, *P. Natl. Acad. Sci. USA*, 116, 1095–1103, 2019.
- Rintoul, S. R., Silvano, A., Pena-Molino, B., van Wijk, E., Rosenberg, M., Greenbaum, J. S., and Blankenship, D. D.: Ocean heat drives rapid basal melt of the Totten Ice Shelf, *Sci. Adv.*, 2, e1601610, 2016.
- Ritz, C., Edwards, T. L., Durand, G., Payne, A. J., Peyaud, V., and Hindmarsh, R. C. A.: Potential sea-level rise from Antarctic ice-sheet instability constrained by observations, *Nature*, 528, 115–118, 2015.
- Scherer, R. P., DeConto, R. M., Pollard, D., and Alley, R. B.: Wind-blown Pliocene diatoms and East Antarctic Ice Sheet retreat, *Nat. Commun.*, 7, 12957, 2016.
- Scherler, D., Leprince, S., and Strecker, M. R.: Glacier-surface velocities in alpine terrain from optical satellite imagery - Accuracy improvement and quality assessment, *Remote Sens. Environ.*, 112, 3806–3819, 2008.
- Schoof, C.: Ice sheet grounding line dynamics: Steady states, stability, and hysteresis, *J. Geophys. Res.-Earth*, 112, F03S28, 2007.
- Schröder, L., Horwath, M., Dietrich, R., Helm, V., van den Broeke, M. R., and Ligtenberg, S. R. M.: Four decades of Antarctic surface elevation changes from multi-mission satellite altimetry, *The Cryosphere*, 13, 427–449, <https://doi.org/10.5194/tc-13-427-2019>, 2019.
- Shen, Q., Wang, H. S., Shum, C. K., Jiang, L. M., Hsu, H. T., and Dong, J. L.: Recent high-resolution Antarctic ice velocity maps reveal increased mass loss in Wilkes Land, East Antarctica, *Sci. Rep.-UK*, 8, 4477, 2018.
- Stokes, C. R., Sanderson, J. E., Miles, B. W. J., Jamieson, S. S. R., and Leeson, A. A.: Widespread distribution of supraglacial lakes around the margin of the East Antarctic Ice Sheet, *Sci. Rep.-UK*, 9, 13823, 2019.
- Thoma, M., Jenkins, A., Holland, D., and Jacobs, S.: Modelling Circumpolar Deep Water intrusions on the Amundsen Sea continental shelf, Antarctica, *Geophys. Res. Lett.*, 35, L18602, 2008.
- Treasure, A. M., Roquet, F., Ansoorge, I. J., Bester, M. N., Boehme, L., Bornemann, H., Charrassin, J.-B., Chevallier, D., Costa, D. P., Fedak, M. A., Guinet, C., Hammill, M. O., Harcourt, R. G., Hindell, M. A., Kovacs, K. M., Lea, M.-A., Lovell, P., Lowther, A. D., Lydersen, C., McIntyre, T., McMahan, C. R., Muelbert, M. M. C., Nicholls, K., Picard, B., Reverdin, G., Trites, A. W., Williams, G. D., and de Bruyn, P. J. N.: Marine mammals exploring the oceans pole to pole: a review of the MEOP consortium, *Oceanography*, 30, 132–138, 2017.
- Trusel, L. D., Frey, K. E., Das, S. B., Karnauskas, K. B., Munneke, P. K., van Meijgaard, E., and van den Broeke, M. R.: Divergent trajectories of Antarctic surface melt under two twenty-first-century climate scenarios, *Nat. Geosci.*, 8, 927–932, 2015.
- Vogel, C. R.: Computational methods for inverse problems, 23, Siam, Philadelphia, 2002.
- Weertman, J.: Stability of the junction of an ice sheet and an ice shelf, *J. Glaciol.*, 13, 3–11, 1974.
- Williams, T., van de Flierdt, T., Hemming, S. R., Chung, E., Roy, M., and Goldstein, S. L.: Evidence for iceberg armadas from East Antarctica in the Southern Ocean during the late Miocene and early Pliocene, *Earth Planet. Sc. Lett.*, 290, 351–361, 2010.
- Young, D. A., Wright, A. P., Roberts, J. L., Warner, R. C., Young, N. W., Greenbaum, J. S., Schroeder, D. M., Holt, J. W., Sugden, D. E., Blankenship, D. D., van Ommen, T. D., and Siegert, M. J.: A dynamic early East Antarctic Ice Sheet suggested by ice-covered fjord landscapes, *Nature*, 474, 72–75, 2011.
- Young, D. A., Lindzey, L. E., Blankenship, D. D., Greenbaum, J. S., de Gorod, A. G., Kempf, S. D., Roberts, J. L., Warner, R. C., Van Ommen, T., Siegert, M. J., and Le Meur, E.: Land-ice elevation changes from photon-counting swath altimetry: first applications over the Antarctic ice sheet, *J. Glaciol.*, 61, 17–28, 2015.